J. Fluid Mech. (1997), *vol.* 343, *pp.* 131–151. Printed in the United Kingdom

© 1997 Cambridge University Press

Topographically forced long waves on a sheared coastal current. Part 1 The weakly nonlinear response

By S. R. CLARKE AND E. R. JOHNSON

Department of Mathematics, University College London, Gower St, London WC1E 6BT, UK

(Received 23 April 1996)

The flow of a constant-vorticity current past coastal topography is investigated in the long-wave weakly nonlinear limit. In contrast to other near-critical weakly nonlinear systems this problem does not exhibit hydraulically controlled solutions. It is shown that near criticality the evolution of the vorticity interface is governed by a forced BDA (Benjamin–Davis–Acrivos) equation. The solutions of this equation are discussed and two distinct near-critical flow regimes are identified. Owing to the non-local nature of the forcing, the first of these regimes is characterized by quasi-steady solutions controlled at the topography with some blocking of the upstream rotational fluid, while in the second regime steady nonlinear wavetrains form downstream of the obstacle with no upstream influence. In the hydraulic limit the velocity band for both of these critical regimes approaches zero.

1. Introduction

The problem of hydraulic control of rotating channel flows has received much attention over the last few decades owing to its obvious importance in understanding exchange flows through the straits and sills of the world's oceans. A review of the problem of hydraulic control by Kelvin waves is presented by Pratt & Lundberg (1991). Recent work has extended this and investigated the importance of hydraulic control in other geophysical flows. For example, hydraulic control by Rossby waves has been studied by Pratt & Armi (1987), Woods (1993) and Haynes, Johnson, & Hurst (1993), while Hughes (1985*a*, *b*, 1986*a*, *b*, 1987, 1989) has studied hydraulic control by coastally trapped waves. These flows are controlled where the topographic perturbation is a maximum with subcritical flow upstream and supercritical flow downstream. The solution at a given point away from the control is then determined simply by the strength of the topographic perturbation there.

Hydraulic theories in general require that the flow is steady and the along-flow lengthscale is arbitrarily long. To avoid these limitations Stern (1991) used a modified contour dynamics method to investigate the blocking of a simple sheared coastal current by a cape. He was specifically interested in the possibility of flow reversal, which he argued would invalidate the hydraulic approximation (although later work by Haynes *et al.* 1993 shows this is not necessarily so). His solutions demonstrate some hydraulic features, such as finite length narrowing downstream of the cape and the possibility of upstream influence. They also show that eddies form downstream and, in some cases (see his figures 8, 10 and 12), the suggestion of a large-amplitude wave upstream. Neither of these features is predicted by hydraulic theories. Haynes

https://doi.org/10.1017/S0022112097005685 Published online by Cambridge University Press

et al. (1993) also used contour dynamical integrations to investigate the validity of the hydraulic approximation, and in general found good agreement in their geometry.

Simulations like these (Stern 1991; Haynes *et al.* 1993) are limited to inviscid flows with piecewise-constant vorticity. An alternative approach to investigate the validity of the hydraulic approximation is to relax the long-wave approximation and introduce leading-order dispersion and unsteadiness. Grimshaw (1987) used this method to investigate the resonant generation of coastally trapped waves, a similar problem to that studied by Hughes (1985*a*, *b*, 1986*a*, *b*, 1987, 1989) using hydraulic theory. Grimshaw (1987) found a resonant band with evidence of hydraulic control. This approach has the advantages that it is much more generally applicable than contour dynamics, i.e. the vorticity no longer need be piecewise continuous and effects such as bottom friction can be easily incorporated, and the numerical solution speed is at least an order of magnitude faster that contour dynamical simulations. The major disadvantages are that only long waves are treated and, in general, only weak nonlinearity can be incorporated.

This paper applies the approach of Grimshaw (1987) to one of the problems studied by Stern (1991). We consider a sheared coastal current propagating past outcropping topography. In the external ocean region the fluid is irrotational and approaches a constant velocity at large distances from the coast. In the other flow geometry of Stern (1991) in general the outer fluid was allowed to be rotational, but the velocity at the coast was forced to be zero. Although the integrations Stern presents are not carried to long enough times for the flows to have become steady, his results appear to show that downstream of a headland or outcrop a coastal current can return to being of constant width, albeit of a different value from its upstream width. Stern referred to this as blocking of the shear flow, and suggested that this blocking is due to weak hydraulic effects, where long waves are able to propagate upstream. The works described above, with variable bottom topography, allow hydraulic control, and so §2 examines whether hydraulically controlled solutions are possible for the present geometry. It is shown that conservation of vorticity requires that any steady hydraulically controlled solutions, with the current having different widths upstream and downstream of the topography, has reversed flow upstream. However, it is further shown that although two conjugate flow states, one subcritical and the other supercritical, exist a smooth transition from one to the other is impossible. The question arises as to what then is the behaviour of the flow and the remainder of the paper addresses this. Thus the flow upstream of the topography is taken to be reversed subcritical flow with a conjugate unidirectional downstream supercritical flow that is however not smoothly attainable. Numerical integrations and analytical limiting solutions are presented to describe the actual flow evolution in the weakly nonlinear near-critical limit.

The precise flow considered here is a coastal flow that is uniform outside a boundary region where it has constant shear. The width of the boundary region gives the basic length scale of the problem and the magnitude of the shear gives both a time scale and, combined with the length scale, a reference speed for the flow. The geometry is then described by two parameters ϵ and μ, with ϵ measuring the offshore extent of the cape and μ^{-1} its along-coast length scale. A third, dynamical, parameter Δ gives the unperturbed flow speed at the coast and also is the Doppler-shifted wave speed for perturbations of the interface between the sheared and unsheared flow. The dynamical behaviour is of most interest near $\Delta = 0$ where the long-wave speed vanishes. Analytical progress is possible for small capes ($\epsilon \ll 1$), and so the present paper concentrates on the weakly nonlinear near-critical limit of $|\Delta| \ll 1, \epsilon \ll 1$.

https://doi.org/10.1017/S0022112097005685 Published online by Cambridge University Press

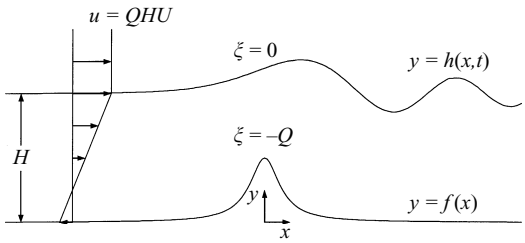


FIGURE 1. A schematic of the flow geometry under consideration. In the coastal region the flow has vorticity $-Q$, while in the outer ocean the flow is irrotational and approaches a uniform along-shore velocity in the far field.

The effects of finite ϵ and Δ are discussed in Part 2 (Clarke & Johnson 1997). In §3 a general evolution equation for this problem is derived following the approach of Grimshaw (1987). In the near-critical limit the equation reduces to a forced BDA equation. In §4 approximate solutions of the forced BDA equation are considered, while in §§5 and 6 steady and unsteady solutions are considered. The implications of these solutions are discussed in §7.

2. Steady hydraulic flows

Consider an inviscid sheared constant-depth current flowing past coastal topography as shown in figure 1. Take the flow to be bounded by a rigid upper surface so that the governing equation is the two-dimensional conservation of the vertical component of vorticity. Let the flow offshore of the current be irrotational, approaching a uniform along-coast flow at large distances from the coast. Let the current have undisturbed width H and vorticity $-Q$ (with $Q > 0$). The behaviour for flows with positive vorticity follow by making the transformation $x \to -x$ and $\zeta \to -\zeta$, where x and ζ are the along-shore coordinate and vertical component of vorticity respectively. Scale the Cartesian coordinates x and y on H, the time t on Q^{-1} and the streamfunction ψ on QH^2. Let the coastline in the far field coincide with $y = 0$, for the offshore coordinate y. The outcropping topography along the vertical coastal wall, $f(x)$, thus satisfies

$$\lim_{|x|\to\infty} f = 0. \tag{1}$$

Denote the interface between the sheared coastal current and the irrotational outer flow by $h(x,t)$. Then ψ satisfies

$$\nabla^2\psi = \begin{cases} 0 & \text{if} \quad y > h(x,t) \\ -1 & \text{if} \quad f(x) < y < h(x,t), \end{cases} \tag{2a}$$

with the matching conditions in the far field

$$\lim_{y\to\infty} \psi = -Uy, \tag{2b}$$

$$\lim_{|x|\to\infty} h = 1, \tag{2c}$$

and no flow across the solid boundary

$$\psi(x, f(x), t) = 0. \tag{2d}$$

https://doi.org/10.1017/S0022112097005685 Published online by Cambridge University Press

The vorticity interface is a material surface and thus at $y = h$,

$$h_t = \frac{\mathrm{d}}{\mathrm{d}x}\{\psi(x, h, t)\}. \tag{2e}$$

Let the topography be characterized by a dimensionless width ϵ and dimensionless lengthscale μ^{-1}. There are thus three parameters of this system: ϵ, μ and U, the exterior velocity. Now consider the steady flow in the limit $\mu \to 0$, with $U = 1$ (i.e. the undisturbed velocity is zero at the boundary).

Divide the domain into two regions, an inner and an outer region, which must be matched across $y = Y$, where Y is a constant such that $h < Y$ and $Y = O(1)$. In the inner region the along-shore motion has a lengthscale of order μ^{-1}. Thus introduce a long spatial coordinate

$$\chi = \mu x, \tag{3}$$

and the streamfunction is, to $O(\mu^2)$,

$$\psi = \begin{cases} -y + D(\chi) & \text{if} \quad y \geqslant h(\chi) \\ -\frac{1}{2}(y-f)^2 + C(\chi)(y-f) & \text{if} \quad y \leqslant h(\chi). \end{cases} \tag{4}$$

To leading order the streamfunction satisfies the far-field boundary condition, therefore the outer flow need not be considered here. The functions D and C are found by enforcing continuity of ψ and ψ_y across $y = h(\chi)$, and so

$$C = h - f - 1, \quad D = \tfrac{1}{2}(h-f)^2 + f. \tag{5a,b}$$

The mass flux in the shear layer is

$$F = -\psi(h) = -\tfrac{1}{2}(h-f)^2 + h - f, \tag{6}$$

and since this is constant

$$h - f = 1 \pm (1 - 2F)^{1/2}. \tag{7}$$

Hydraulically controlled flows can only exist if for particular F there are two non-negative and unequal solutions of (7), thus F must satisfy

$$0 \leqslant F < \tfrac{1}{2}. \tag{8}$$

The velocity at any point on the coast can then take only one of the two values

$$u_{1,2} = \pm(1 - 2F)^{1/2}, \tag{9}$$

independently of f, the size of the topographic perturbation. This has two important implications. First, since for hydraulic control the flow is subcritical upstream and supercritical downstream and since the velocity at the interface is unity, a necessary condition for hydraulic control is that there is reversed flow upstream. This agrees with Stern's hydraulic analysis for a finite-width channel. Second, since the speed at the wall can take only one of the two distinct values (9), independently of f, there can be no smooth transition from subcritical to supercritical flow. Conjugate flows exist but cannot merge smoothly at a control. The only mechanism by which two conjugate flows could merge would be through a stationary rearward-facing shock over the topography. This however invalidates the hydraulic approximation.

Having established that smooth hydraulically controlled flow does not occur in this geometry, our interest is to determine whether weak-hydraulic flows are possible, where conjugate flows exist upstream and downstream and an abrupt or unsteady

https://doi.org/10.1017/S0022112097005685 Published online by Cambridge University Press

transition occurs over the topography. For these flows to exist it is clear that there must be a flow reversal upstream of the topography and therefore it is convenient to consider flows which already possess a flow reversal and U is not necessarily unity.

3. Weakly nonlinear evolution equations

Some analytical progress can be made by considering unsteady long-wave solutions of the problem (2), taking $\mu \ll 1$. This is a limit of the problem considered by Grimshaw (1987), and in the weakly nonlinear limit, $\epsilon = O(\mu)$, it would be expected that the response of the interface will be $O(\epsilon^{1/2})$ and a resonant regime will result. However, restricting the fluid to be of constant depth and permitting only coastline variations (which as noted by Grimshaw is equivalent to assuming that the width of the shear current is greater than the width of the continental shelf) makes the forcing in Grimshaw's equation identically zero, so forcing and nonlinearity do not balance at leading order. Thus, for the special case of a constant-depth fluid an alternative scaling for the wave response is needed. Note that this is not dependent in any way on the form of the imposed current. A similar derivation to that below could be performed for currents with a continuous variation in vorticity.

The inner and outer regions are now separated by the interface $y = h(x,t)$. In the inner coastal region the offshore motion has lengthscale of order unity, while the along-shore motion again has lengthscale of order μ^{-1}. This suggests that the timescale for wave propagation on the interface is also order μ^{-1}. Thus introduce χ, defined by (3), and a new temporal coordinate

$$T = \mu t. \tag{10}$$

Then in the inner region ψ satisfies

$$\psi_{yy} + \mu^2 \psi_{\chi\chi} = -1, \tag{11}$$

which, to satisfy (2*d*), has the solution

$$\begin{aligned}\psi = &-\tfrac{1}{2}(y-f)^2 + C(y-f)\\ &+\mu^2\left(-\tfrac{1}{6}(f+C)_{\chi\chi}(y-f)^3 + \tfrac{1}{2}(y-f)^2\left(f_\chi^2 + 2C_\chi f_\chi + c f_{\chi\chi}\right)\right) + O(\mu^4),\end{aligned} \tag{12}$$

where $C(\chi, T)$ is the, as yet undetermined, speed at the coast.

In the outer region both the offshore and along-shore lengthscales are of order μ^{-1}. Hence introduce

$$\eta = \mu y. \tag{13}$$

The solution for ψ can then be written

$$\psi = -Uy + \frac{1}{2\pi}\int_{-\infty}^{\infty} \hat{M}(k,T)\exp(\mathrm{i}k\chi - |k|\eta)\mathrm{d}k, \tag{14a}$$

for

$$\hat{M}(k,T) = \int_{-\infty}^{\infty} M(\chi,T)\exp(-\mathrm{i}k\chi)\mathrm{d}\chi, \tag{14b}$$

where $M(\chi,T)$ is the, as yet undetermined, perturbation to the streamfunction at the outer edge of the shear flow. Expanding (14) in powers of μ gives that near the interface in the outer region

$$\psi = -Uy + M - \mu y\mathscr{B}\{M\} - \tfrac{1}{2}\mu^2 y^2 M_{\chi\chi} + O(\mu^3), \tag{15a}$$

https://doi.org/10.1017/S0022112097005685 Published online by Cambridge University Press

where

$$\mathscr{B}\{M\} = \frac{1}{2\pi}\int_{-\infty}^{\infty} \hat{M}|k| \exp \mathrm{i}k\chi \, \mathrm{d}k = \frac{1}{\pi}\frac{\partial}{\partial \chi}\fint_{-\infty}^{\infty} \frac{M(y)}{\chi - y}\mathrm{d}y, \tag{15b}$$

and the Hilbert integral in the alternative form for $\mathscr{B}$ is a Cauchy Principal Value.

It remains to find M and C by invoking the continuity of ψ and ψ_y across $y = h(\chi, T)$. At this point the further assumption is made that the dimensionless width of the topography, ϵ, scales as the characteristic wavenumber of the topography, μ. The response of the interface is assumed to be weakly nonlinear and scale as the width of the topography. Therefore introduce

$$f = \alpha\mu\tilde{f}, \quad h - f = 1 + \alpha\mu A, \tag{16a,b}$$

where α is an order-unity parameter measuring the width of the topographic outcrop in units of μ. Dropping the tildes and invoking continuity of ψ and ψ_y across the interface gives

$$-\tfrac{1}{2}(1 + 2\alpha\mu A + \alpha^2\mu^2 A^2) + C(1 + \alpha\mu A) - \tfrac{1}{6}\mu^2 C_{\chi\chi}$$
$$= -U - \alpha\mu U(f + A) + M - \mu\mathscr{B}\{M\} - \tfrac{1}{2}\mu^2 M_{\chi\chi} + O(\mu^3), \tag{17a}$$

$$-1 - \alpha\mu A + C - \tfrac{1}{2}\mu^2 C_{\chi\chi} = -U - \mu\mathscr{B}\{M\} - \mu^2 M_{\chi\chi} + O(\mu^3). \tag{17b}$$

Examination of (17b) shows that to leading order C is constant, consequently the terms of the form $\mu^2 C_{\chi\chi}$ in each of the above equations can be neglected. At leading order $M = \frac{1}{2}$ and the $O(\mu^2)$ terms involving M in each equation can also be neglected. Thus introduce

$$M = \tfrac{1}{2} + \alpha\mu\tilde{M}. \tag{18}$$

It can then be shown that, dropping the tilde,

$$C = 1 - U + \alpha\mu A - \mu^2\mathscr{B}\{M\} + O(\mu^3), \quad M = Uf + A + O(\mu^2). \tag{19a,b}$$

Defining

$$\Delta = U - 1, \tag{20}$$

gives the streamfunction on the interface as

$$\psi(\chi, h(\chi, T), T) = \tfrac{1}{2} - U - \alpha\Delta A + \tfrac{1}{2}\alpha^2\mu^2 A^2 - \alpha\mu^2\mathscr{B}\{(\Delta + 1)f + A\} + O(\mu^3). \tag{21}$$

Then (2e) gives

$$A_T + \Delta A_\chi - \alpha\mu A A_\chi + \mu\mathscr{B}\{(\Delta + 1)f_\chi + A_\chi\} = O(\mu^2). \tag{22}$$

It is possible to envisage many different forms for the initial current width $A(\chi, 0)$. Perhaps the simplest conceptually is that of the topography impulsively forming in a previously uniform shear layer. The outcropping of the obstacle is taken to occur over a timescale much faster than the response time of the fluid, and so

$$h(\chi, 0) = 1, \tag{23a}$$

or

$$A(\chi, 0) = -f(\chi). \tag{23b}$$

In the weakly nonlinear limit considered here, this condition is identical to that used by Stern (1991).

https://doi.org/10.1017/S0022112097005685 Published online by Cambridge University Press

A balance between unsteady and dispersive terms in (22) would suggest that there are two timescales for this problem: the advection time T and a slower time $\tau = \mu T$. Therefore introduce

$$\tau = \mu T. \tag{24}$$

Ignoring terms of $O(\mu^2)$, (22) and (23*b*) give

$$A_T + \mu A_\tau + \Delta A_\chi - \alpha\mu A A_\chi + \mu\mathscr{B}\{(\Delta + 1)f_\chi + A_\chi\} = 0, \tag{25a}$$

with

$$A(\chi, T = 0, \tau = 0) = -f(\chi). \tag{25b}$$

When Δ is order unity the leading-order solution of (25) is a free wave. To demonstrate this a perturbation expansion for A is sought of the form

$$A = A^{(0)} + \mu A^{(1)} + \dots\ . \tag{26}$$

At leading order

$$A^{(0)} = -f(\theta), \tag{27}$$

where $\theta = \chi - \Delta T$ is a phase variable. The next order gives

$$A^{(1)}_T + A^{(0)}_\tau + \Delta A^{(1)}_\chi - \alpha A^{(0)} A^{(0)}_\theta + \mathscr{B}\left\{(\Delta + 1)f_\chi + A^{(0)}_\theta\right\} = 0, \tag{28a}$$

subject to

$$A^{(1)}(\chi, T = 0, \tau = 0) = 0. \tag{28b}$$

Balancing functions of θ gives the evolution equation

$$A^{(0)}_\tau - \alpha A^{(0)} A^{(0)}_\theta + \mathscr{B}\left\{A^{(0)}_\theta\right\} = 0, \tag{29a}$$

with

$$A^{(0)}(\theta, 0) = -f(\theta), \tag{29b}$$

and balancing functions of χ gives

$$A^{(1)} = \frac{(\Delta + 1)}{\Delta}\mathscr{B}\{f(\chi - \Delta T) - f(\chi)\}. \tag{30}$$

Equation (29*a*) is the BDA equation (Benjamin 1967; Davis & Acrivos 1967).

For small Δ the leading-order correction $A^{(1)}$ is

$$A^{(1)} = -T\mathscr{B}\{f_\chi\} + O(\Delta T). \tag{31}$$

Hence for large time the leading-order correction increases without bounds and the perturbation expansion breaks down. Thus the forced wave enters the problem at leading order. This near-critical limit, occurs, in general, when Δ is order μ. In this limit we return to (25) and introduce

$$\Delta = \mu\tilde{\Delta}. \tag{32}$$

Then the advection time T disappears from the leading-order problem and A satisfies, dropping the tilde,

$$A_\tau + \Delta A_\chi - \alpha A A_\chi + \mathscr{B}\{f_\chi + A_\chi\} = 0, \tag{33a}$$

https://doi.org/10.1017/S0022112097005685 Published online by Cambridge University Press

with initial condition

$$A(\chi, 0) = -f(\chi), \tag{33b}$$

a forced BDA (fBDA) equation. Grimshaw (1987) derived a similar equation for coastally trapped waves. In his case the forcing is of the form f_χ, rather than a Hilbert transform, and the equation has a trivial initial condition. As will be seen, this difference in the forcing has important consequences.

For definiteness, the following three Sections concentrate exclusively on the solution of (33), with topography

$$f = \frac{1}{\chi^2 + 1}, \tag{34}$$

and $\alpha > 0$. Consequently only outcrops are considered. The lengthscale and the amplitude of the topography are both $O(1)$ due to the choice of the perturbation parameters. Profile (34) allows some analytical progress; however in general the exact details of the topography are not important.

4. Approximate solutions

4.1. *Linear solutions, $\alpha \ll 1$*

For $\alpha \ll 1$ write

$$A + f = A^{(0)} + O(\alpha). \tag{35}$$

Then $A^{(0)}$ satisfies, to leading order in α,

$$A^{(0)}_\tau + \Delta A^{(0)}_\chi + \mathscr{B}\{A^{(0)}_\chi\} = \Delta f_\chi, \tag{36a}$$

with

$$A^{(0)}(\chi, 0) = 0. \tag{36b}$$

Waves of wavenumber k satisfying (36) have frequency

$$\omega = k(\Delta + |k|). \tag{37}$$

The phase and group velocity of such waves as a function of k are shown in figure 2. When $\Delta < 0$ the frequency and phase velocity vanish at $|k| = -\Delta$ and the group velocity is positive there. Thus forcing generates lee waves to the right of the outcrop. When $\Delta > 0$ the phase velocity has no zeros and no standing waves form.

The Green's function of (36), $G(\chi, \tau)$, will be the solution corresponding to a Dirac-delta function outcrop, $f(x) = \delta(x)$. The full solution for $A^{(0)}$ is then

$$A^{(0)}(\chi, \tau) = \int_{-\infty}^{\infty} f(x) G(\chi - x, \tau) \mathrm{d}x. \tag{38}$$

Standard Fourier transform techniques give the Green's function as

$$G = \frac{\Delta}{\pi} \int_0^\infty \frac{1}{\Delta + k} (\cos k\chi - \cos(k\chi - k(\Delta + k)\tau)) \mathrm{d}k. \tag{39}$$

This integral is typical of forced linear dispersive systems (Patoine & Warn 1982;

https://doi.org/10.1017/S0022112097005685 Published online by Cambridge University Press

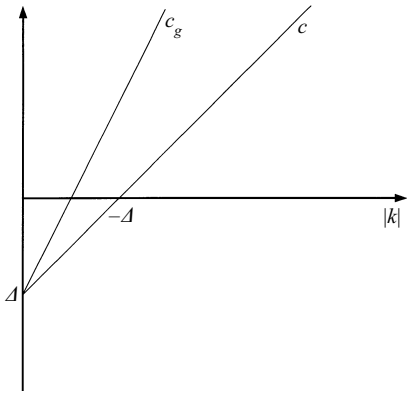


FIGURE 2. The phase velocity, c, and group velocity, c_g, as a function of the wavenumber k, for solutions of the linear fBDA equation, (36), when $\Delta < 0$. When $\Delta > 0$ the phase velocity has no real zeros.

Akylas 1984; Johnson 1985). To evaluate, consider G as the sum of the two integrals

$$G_s = \frac{\Delta}{\pi}\int_0^\infty \frac{1}{\Delta + k}\cos k\chi \, \mathrm{d}k, \tag{40a}$$

$$G_u = -\frac{\Delta}{\pi}\int_0^\infty \frac{1}{\Delta + k}\cos(k\chi - k(\Delta + k)\tau)\mathrm{d}k. \tag{40b}$$

When $\Delta < 0$ each integrand has a pole at $k = -\Delta$, although the integrand in (39) does not.

Consider first $\Delta > 0$, so

$$\begin{aligned} G_s &= (\Delta/\pi)\left\{-\cos|\Delta\chi|\,\mathrm{Ci}\,|\Delta\chi| - \sin|\Delta\chi|\left(\mathrm{Si}\,|\Delta\chi| - \tfrac{1}{2}\pi\right)\right\} \\ &= (\Delta/\pi)g(|\Delta\chi|), \end{aligned} \tag{41}$$

where Ci and Si are the cosine and sine integrals, and $g(z)$ is defined in Abramowitz & Stegun (1972). Figure 3 gives a plot of $g(z)$. Near $z = 0$, g behaves as $O(\log|z|)$. The second integral G_u can be approximated at large times by the method of stationary phase. At large times, to $O(\tau^{-1})$,

$$G_u = \begin{cases} -\dfrac{2\Delta}{\pi^{1/2}(\xi + 2\Delta\tau^{1/2})}\cos\left(\dfrac{\xi^2}{4} - \dfrac{\pi}{4}\right) & \text{if} \quad \xi > 0 \\ -(8\pi\tau)^{-1/2} & \text{if} \quad \xi = 0 \\ 0 & \text{if} \quad \xi < 0. \end{cases} \tag{42}$$

Here $\xi = \tau^{-1/2}(\chi - \Delta\tau)$ is a phase variable and (42) corresponds to a wavetrain with front travelling at speed Δ.

When $\Delta < 0$ the integration path must pass around the poles on the real axis, thus

$$G_s = \Delta\,\mathrm{sgn}(\chi)\sin\Delta\chi - (\Delta/\pi)g(|\Delta\chi|), \tag{43}$$

and

$$G_u = -\Delta\,\mathrm{sgn}(\chi + \Delta\tau)\sin\Delta\chi + G_u^*, \tag{44}$$

where the function G_u^* represents a dispersive wavetrain. This can be evaluated by

https://doi.org/10.1017/S0022112097005685 Published online by Cambridge University Press

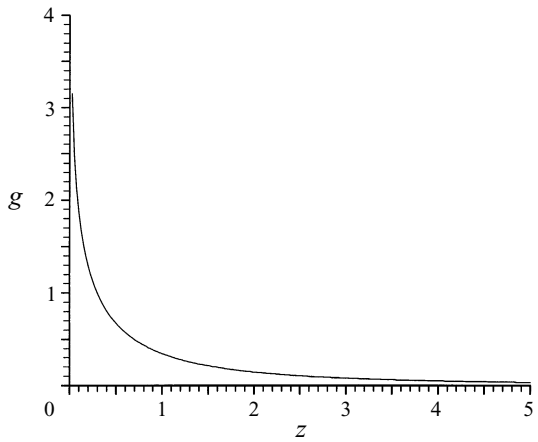


FIGURE 3. The function $g(z)$, (41), which for $\Delta > 0$ is proportional to the steady part of the Green's function for the linear fBDA equation, (36).

deforming the path of integration onto the line $k = r\exp \mathrm{i}\pi/3$, and so

$$G_u^* = -\frac{\Delta}{\pi}\mathrm{Re}\left\{\int_0^\infty \frac{\exp\tfrac{1}{2}(-\sqrt{3}(r(\chi-\Delta\tau)+r^2\tau)+\mathrm{i}(r(\chi-\Delta\tau)-r^2\tau))}{r+\Delta\exp(-\mathrm{i}\pi/3)}\mathrm{d}r\right\}. \tag{45}$$

Then using the method of stationary phase at large times, to $O(\tau^{-1})$,

$$G_u^* = \begin{cases} -\left(\dfrac{8\Delta^2}{\pi(\xi^2+2\xi\Delta\tau^{1/2}+4\Delta^2\tau)}\right)^{1/2}\exp-\dfrac{3^{3/2}\xi^2}{8} & \\ \qquad\times\cos\left(\dfrac{\xi^2}{4}-\dfrac{\pi}{4}-\arcsin\left(\dfrac{3\Delta^2}{\xi^2+2\xi\Delta\tau^{1/2}+4\Delta^2\tau}\right)^{1/2}\right) & \text{if}\quad \xi>0 \\ -(2+3^{1/2})(4\pi\tau)^{-1/2} & \text{if}\quad \xi=0 \\ 0 & \text{if}\quad \xi<0. \end{cases} \tag{46}$$

Combining these results gives

$$G = (\Delta/\pi)g(|\Delta\chi|) + G_d \qquad \text{if} \qquad \Delta > 0, \tag{47}$$

and

$$G = -(\Delta/\pi)g(|\Delta\chi|) + G_u^* + \Delta(\mathrm{sgn}(\chi)-\mathrm{sgn}(\chi+\Delta\tau))\sin\Delta\chi \qquad \text{if} \qquad \Delta < 0. \tag{48}$$

The last term represents a lee-wave train: standing waves with zero phase speed downstream of the topography whose spatial extent grows with the group velocity.

For general topography the dispersive term of the solution behaves for large times as $O(\tau^{-1/2})$ and hence can be ignored. The long-term solutions are therefore

$$A^{(0)} = \frac{\Delta}{\pi}\int_{-\infty}^{\infty} f(x)g(|\Delta(\chi-x)|)\mathrm{d}x \qquad \text{if} \qquad \Delta > 0 \tag{49}$$

and

$$A^{(0)} = -\frac{\Delta}{\pi}\int_{-\infty}^{\infty} f(x)g(|\Delta(\chi-x)|)\mathrm{d}x + 2\Delta\int_{\chi+\Delta\tau}^{\chi} f(x)\sin\Delta(\chi-x)\mathrm{d}x \qquad \text{if} \qquad \Delta < 0. \tag{50}$$

https://doi.org/10.1017/S0022112097005685 Published online by Cambridge University Press

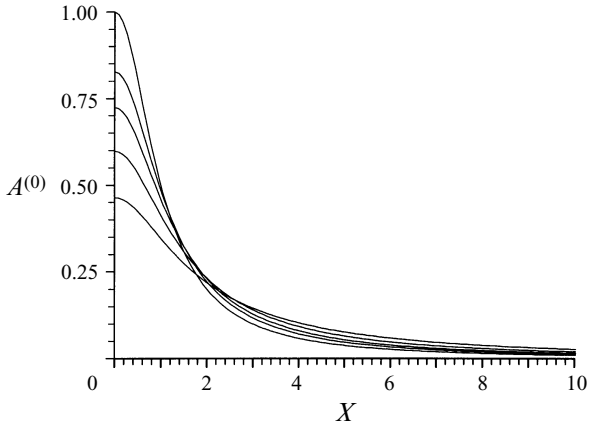


FIGURE 4. The localized solution to the linear fBDA equation, (36), in the vicinity of the topography (34). The solution, (49), is symmetric about $\chi = 0$ and is shown for $\Delta = 0.5, 1, 2$ and 4 and $\Delta \to \infty$, where $A^{(0)}(0)$ increases as Δ increases. Note that $\Delta \to \infty$ corresponds to $A^{(0)} \equiv f$.

Consider the flow in the vicinity of the topography. For $\Delta \neq 0$ it can be shown that

$$\int_{-\infty}^{\infty} A^{(0)} \mathrm{d}\chi = \int_{-\infty}^{\infty} f \ \mathrm{d}\chi. \tag{51}$$

This localized solution is shown in figure 4 for the topography (34) and various values of Δ. As $|\Delta|$ becomes large $A^{(0)} \to f$, as required by (36*a*). As $|\Delta|$ becomes smaller the effect of dispersion increases giving a wave of smaller amplitude but increased wavelength.

For symmetric topography the lee-wave contribution when $\Delta < 0$ reduces to

$$A^{(0)} \approx \Delta[\mathrm{sgn}(\chi) - \mathrm{sgn}(\chi + \Delta\tau)]\hat{f}(\Delta) \sin \Delta\chi, \tag{52}$$

where $\hat{f}(k)$ is the Fourier transform of f. For (34) the lee-wave amplitude is $2\pi\Delta \exp \Delta$ which has a maximum of $2\pi/e$ at $\Delta = -1$. Comparing this expression with figure 4 shows that when $\Delta < 0$ and $|\Delta| \sim 1$ the flow is dominated by lee waves, whereas for $|\Delta| \gg 1$ the flow is dominated by the perturbation in the vicinity of the topography.

These features of the linear solutions are shown in figure 5 for two solutions of (36) and the topography (34). In the supercritical flow the solution consists of the perturbation in the vicinity of the obstacle and the downstream-propagating wavetrain. For subcritical flow the solution becomes significantly more complicated due to the interaction of the various parts; however each part is still apparent. The flow upstream of the obstacle is dominated by the wavetrain with front propagating at speed Δ and downstream of the obstacle the lee-wave train extends at rate $-\Delta$. This is terminated by a slow decay rather than the step-function of the Green's function. The modulation of the lee waves is due to interactions with the dispersive wavetrain. In the vicinity of the outcrop the steady perturbation to the interface is superimposed on the lee waves and dispersive wavetrain.

Finally, when $\Delta = 0$, (36) implies that $A^{(0)} \equiv 0$. Even for Δ arbitrarily small the solutions remain bounded for all time. This behaviour contrasts with typical forced resonant wave problems, where if nonlinear effects are neglected the solution becomes unbounded at large time.

https://doi.org/10.1017/S0022112097005685 Published online by Cambridge University Press

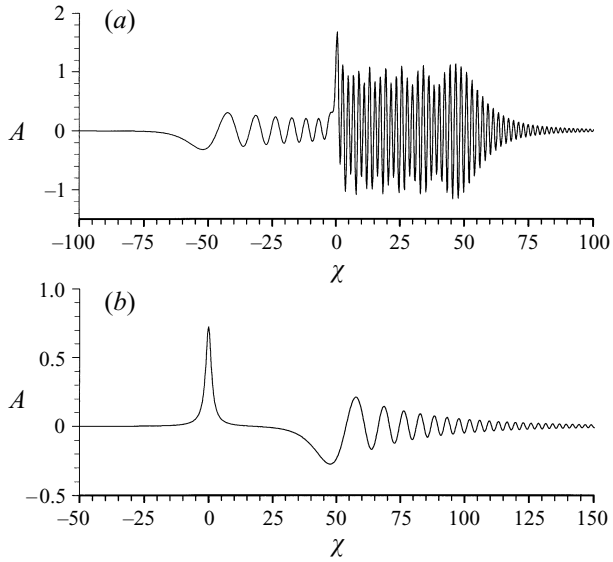


FIGURE 5. Solutions of the linear fBDA equation, (36), for the topography (34) at time $\tau = 20$. (*a*) A subcritical solution where $\Delta = -3$ and, (*b*) a supercritical solution with $\Delta = 2$.

4.2. *The hydraulic approximation,* $\alpha \gg 1$

For large α dispersive effects can be expected to be negligible at least over time intervals short compared to the time τ, and on these timescales the fBDA equation will be dominated by nonlinear effects. Thus write

$$A = A^{(0)} + O(\alpha^{-1}), \quad \Delta = \alpha V, \quad \alpha\tau = \sigma. \tag{53a–c}$$

Then $A^{(0)}$ satisfies

$$A^{(0)}_{\sigma} + VA^{(0)}_{\chi} - A^{(0)}A^{(0)}_{\chi} = O(\alpha^{-1}), \tag{54a}$$

with

$$A^{(0)}(\chi, 0) = -f(\chi). \tag{54b}$$

System (54) has the solution

$$A^{(0)} = -f(\chi_0), \tag{55a}$$

where

$$\chi - \chi_0 - (V + f(\chi_0))\sigma = 0. \tag{55b}$$

Because f and A are chosen to have the same length and width scales there is no forcing to leading order: an $O(\epsilon)$ forcing produces an $O(\epsilon)$ response. One indication of hydraulic control in forced resonant weakly nonlinear systems is that in the hydraulic approximation at long times an expansion fan forms at the maximum of the topography (Grimshaw & Smyth 1986; Haynes *et al.* 1993). Consequently a steady solution forms with unequal limits upstream and downstream and the perturbation amplitude is solely dependent on the amplitude of the topography. In the case considered here there is no expansion fan in the hydraulic approximation and so the flow cannot be hydraulically controlled.

https://doi.org/10.1017/S0022112097005685 Published online by Cambridge University Press

For the headland (34), solution (55) develops a critical gradient at $\sigma = 3^{1/2}$. In some hydraulic systems solutions can be extended to larger times by introducing shocks; however within the present model it is the neglected dispersive term, $\mathscr{B}\{A_\chi\}$, that becomes important in the neighbourhood of the jump. Integrations presented later show that a non-monotonic transition forms between two regions of constant but differing amplitude. Subsequently, these wave-like transition regions are described as undular bores. Over larger timescales where τ is order unity the previously neglected forcing term becomes important.

5. Steady solutions

In describing the behaviour of the flow for various values of the two parameters α and Δ, it is convenient to first determine those values of α and Δ for which the flow in the neighbourhood of the topographic outcropping becomes steady at large time. The development of these flows consists solely of the dispersion of the initial transient wave field to leave behind the steady isolated solution.

Suppose that at large time A becomes steady and the sheared flow has constant width far from the outcrop, such that

$$\lim_{\chi\to-\infty} A = A_u, \qquad \lim_{\chi\to\infty} A = A_d. \tag{56}$$

Integrating the steady form of (33) once gives

$$\Delta A - \tfrac{1}{2}\alpha A^2 + \mathscr{B}\{f + A\} = \Delta A_u - \tfrac{1}{2}\alpha A_u^2. \tag{57}$$

Since this is invariant under the transformation

$$A \to A + A_u, \quad \Delta \to \Delta + A_u, \tag{58a,b}$$

it is sufficient to take $A_u = 0$, so steady isolated solutions of (33) satisfy

$$\Delta A - \tfrac{1}{2}\alpha A^2 + \mathscr{B}\{f + A\} = 0. \tag{59}$$

This restricts the possible values of the downstream shear current width, A_d, to either one of the two values

$$A_d = 0 \quad \text{or} \quad A_d = 2\Delta/\alpha. \tag{60}$$

Integrating (59) once gives

$$\int_{-\infty}^{\infty} A\left(\frac{2\Delta}{\alpha} - A\right) \mathrm{d}\chi = 0. \tag{61}$$

The only continuous function non-negative over an interval whose integral vanishes is the zero function. Hence, the integrand is either negative somewhere, and so the solution is not monotone, or A is identically zero or $2\Delta/\alpha$. There are thus no steady smooth monotone solutions joining differing upstream and downstream values of A. This contrasts with equivalent conditions for the fKdV equation of Grimshaw & Smyth (1986) or the fBDA equation of Grimshaw (1987). In both of these cases when steady transition solutions exist the integral corresponding to (61) is strictly positive, allowing A to vary monotonically. It thus appears that, even when dispersion is included and independently of α, steady transition solutions cannot exist for the problem considered here. This extends the result derived in §2 under the hydraulic approximation.

https://doi.org/10.1017/S0022112097005685 Published online by Cambridge University Press

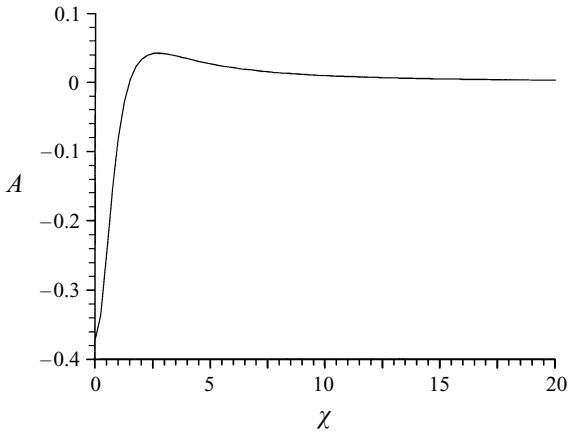


FIGURE 6. A solution of the steady fBDA equation, (59), and the topography (34) for $\alpha = \Delta = 1$. The solution is symmetric about $\chi = 0$.

For f given by (34) steady rational solitary wave solutions of (59) can be constructed, where

$$A = \frac{\beta}{\chi^2 + 1}, \tag{62}$$

provided α and β satisfy

$$\alpha = 4\Delta(\Delta - 1), \quad \beta = 4\Delta. \tag{63a,b}$$

Of the two branches of this solution for $\alpha \geqslant 0$, only those for which Δ is negative are of interest, as for the initial condition (33b) solutions on the other branch are not physically realizable. This can be easily seen by noting that, in the limit $\alpha \to 0$, the rational solitary waves on the negative branch are in agreement with the linear unsteady solution, whereas those on the positive branch contradict the linear unsteady solution.

If $\Delta = 0$ (61) implies that $A \equiv 0$. This however is not a solution of (59) with non-trivial f. Thus steady isolated solutions are not possible for $\Delta = 0$.

When Δ is strictly positive the Fourier transform method described in the Appendix converges to isolated solutions for all values of Δ provided the solution domain and number of collocation points is sufficiently large. Figure 6 gives an example of these solutions for the outcrop (34). As was found for the linear solutions, $A + f$ is a dispersed form of f; however $A + f$ no longer has the same area as f. The steady forms for other values of α and Δ are very similar and so are not shown. The characteristic features of the behaviour of A are that as α is increased the maximum value of A remains approximately constant, while the minimum value of A, i.e. $A(0)$, increases. When Δ is increased both the minimum and maximum values of A decrease in absolute magnitude, while the characteristic length of A also decreases.

For Δ negative the Fourier transform method converges only to periodic solutions, with waves both upstream and downstream of the outcrop having wavenumber of order $|\Delta|$. These are not physically realizable solutions of the initial value problem (33), as the group velocity for infinitesimal waves does not allow upstream wakes. If however a small amount of diffusion is included solutions with a decaying lee-wave train downstream of the cape and no waves upstream can be obtained, which suggests that steady nonlinear lee-wave solutions are possible for negative Δ. For the special

https://doi.org/10.1017/S0022112097005685 Published online by Cambridge University Press

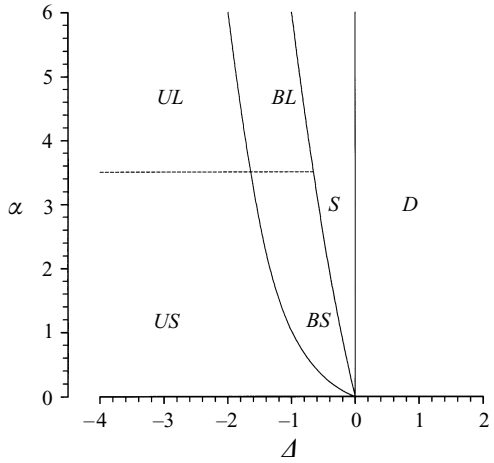


FIGURE 7. A classification of the numerical solutions of the fBDA equation, (33), and the topography (34). The supercritical (downstream-propagating) regime is denoted by D, the steady-critical regime by S, the large- and small-amplitude subcritical (upstream-propagating) regimes by UL and US respectively, and the large- and small-amplitude blocked subregimes by BL and BS respectively.

case where $\alpha = 4\Delta(1-\Delta)$ and no damping the amplitude of the waves away from the topography is zero, and the numerical method converges to the rational solitary wave solution, (62).

6. Unsteady solutions

The analytical and steady approximations of the preceding Sections provide an insight into the behaviour of (33) in the various regimes of the α–Δ parameter space. To discuss the behaviour in other regimes it is necessary to solve the unsteady initial value problem numerically. An efficient method of solution of (33) follows by adapting the pseudo-spectral method of Fornberg & Whitham (1978). This method uses Fourier transforms in space to evaluate the derivatives and integral terms, and a third-order Runge–Kutta method for the time stepping. The topography (34) is used for these solutions. Other shapes have been considered, including asymmetric topography; however these do not significantly alter the general features. The results from the numerical integrations appear to fall into the various classes shown in figure 7. Solutions can be divided into four broad regimes: supercritical, subcritical, blocked and steady critical. The subcritical and blocked regimes each divide further into small- and large-amplitude subregimes.

The supercritical regime occurs for $\Delta > 0$, and is characterized by the long-time solution in the vicinity of the forcing being dominated by an isolated wave. The main characteristics are similar to the hydraulic solution with an undular bore forming downstream of the topography and then being advected away together with its associated rarefaction. In the vicinity of the forcing an isolated wave evolves, which eventually becomes steady. These isolated waves agree closely with the $\Delta > 0$ steady solutions of §5.

The steady-critical regime occupies the region

$$\Delta_c \leqslant \Delta \leqslant 0, \tag{64a}$$

https://doi.org/10.1017/S0022112097005685 Published online by Cambridge University Press

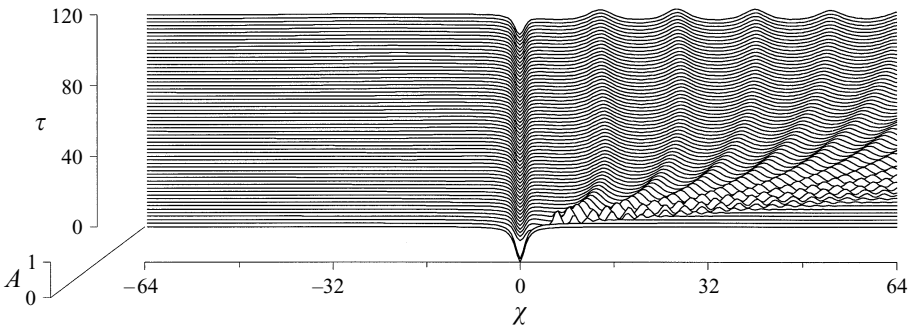


FIGURE 8. A critical solution of the fBDA equation, (33), and the topography (34), where $\Delta = -0.5$ and $\alpha = 4$. Note that only a section of the full solution domain is shown.

where

$$\Delta_c = 1 - \left(1 + \tfrac{1}{2}\alpha\right)^{1/2} \tag{64b}$$

is the negative solution of (63*a*). Figure 8 shows a typical evolution in this regime. An undular bore forms downstream of the outcrop; however in contrast to the supercritical flow the bore and its rarefaction do not propagate. A region of almost-constant-width shear current, subsequently described as a shelf, forms immediately downstream of the outcrop. Here the shelf is negative showing that the sheared region narrows for a distance of order ten obstacle widths before returning to its original width through the undular bore. At later time the speed of individual waves that terminate the shelf decreases: in figure 8 the leading wave has almost become steady by time $\tau = 40$. It appears that all waves that constitute the undular bore become steady at sufficiently large time and a steady nonlinear periodic wavetrain forms on the shelf. No integrations in the critical regime show the leading wave reversing to propagate upstream. Near the outcrop a localized wave forms with only one extremum. The function $A + f$ at the topography thus has smaller amplitude than f, but the same lengthscale. As in the supercritical regime, no waves propagate upstream.

For large α the (empirically determined) limits of the blocked regime are

$$\Delta_c - 1 \leqslant \Delta \leqslant \Delta_c. \tag{65}$$

Figure 9 shows typical behaviour for the large- and small-amplitude subregimes of the blocked regime. An undular bore initially forms downstream of the topography, but eventually the leading wave reverses direction and propagates back towards the topography. The interaction of this wave with the topography generates solitary waves that radiate upstream. At large times careful examination of the numerical solutions shows that there is a weak mean positive upstream influence in the wake of the solitary waves. A shelf, terminated by a downstream-propagating undular bore, forms downstream. It appears that this shelf will extend arbitrarily far downstream at large time. An example of a solution exhibiting these features is shown in figure 10. In the small-amplitude subregime of figure 9(*a*) the characteristic feature of the solution is that it remains unsteady throughout the domain: small-amplitude waves are periodically formed immediately downstream of the topography. These shed waves are split into two: an upstream-propagating wave and a smaller-amplitude wave that propagates downstream on the shelf. In the large-amplitude subregime of figure 9(*b*) the flow becomes steady in an increasingly large region immediately

https://doi.org/10.1017/S0022112097005685 Published online by Cambridge University Press

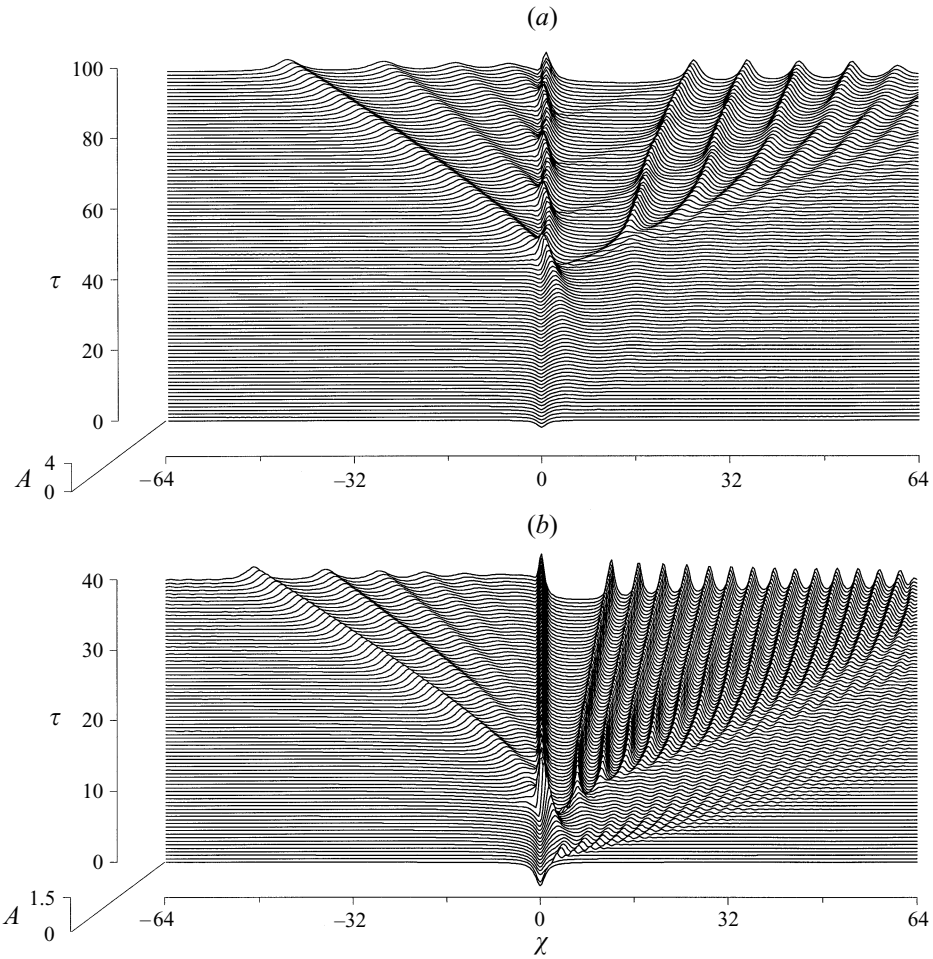


FIGURE 9. Two blocked solutions of the fBDA equation, (33), and the topography (34): (*a*) small-amplitude solution where $\Delta = -0.5$ and $\alpha = 1$, and (*b*) large-amplitude solution where $\Delta = -1.5$ and $\alpha = 4$. Note that only a section of the full solution domain is shown in (*a*).

downstream of the outcrop. Nonlinear effects are sufficiently large to damp wave shedding from the downstream side of the outcrop. However, small-amplitude waves are now periodically generated immediately upstream of the outcrop, and it appears that a uniform-amplitude propagating wavetrain will eventually form upstream of the topography. This flow appears to be evolving to an almost hydraulically controlled flow with subcritical upstream conditions and supercritical downstream conditions. The transition across the outcrop generates small-amplitude waves which propagate upstream.

The mechanism for the unsteady generation of waves at the topography can be seen as being due to the non-local nature of the forcing. For an outcrop with a single maximum as given by (34), the effective forcing function $\mathscr{B}\{f\}$ has three extrema with its maximum at the centre. The main forcing occurs at this maximum, with however smaller-scale forcing at the two side extrema, generating small-amplitude waves at large time.

Figure 11 shows typical flows in the subcritical regime. A wavetrain propagates

https://doi.org/10.1017/S0022112097005685 Published online by Cambridge University Press

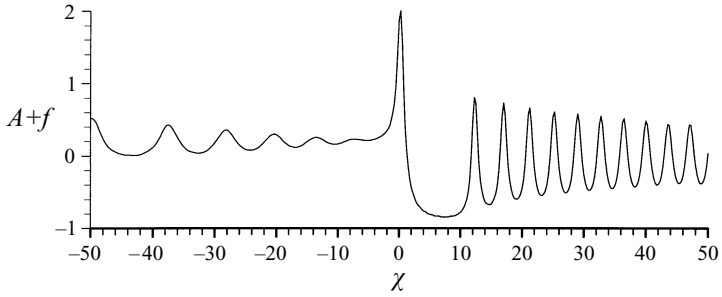


FIGURE 10. The interface shape, $A + f$, from figure 9(b) at $\tau = 40$. Only a section of the solution domain is shown.

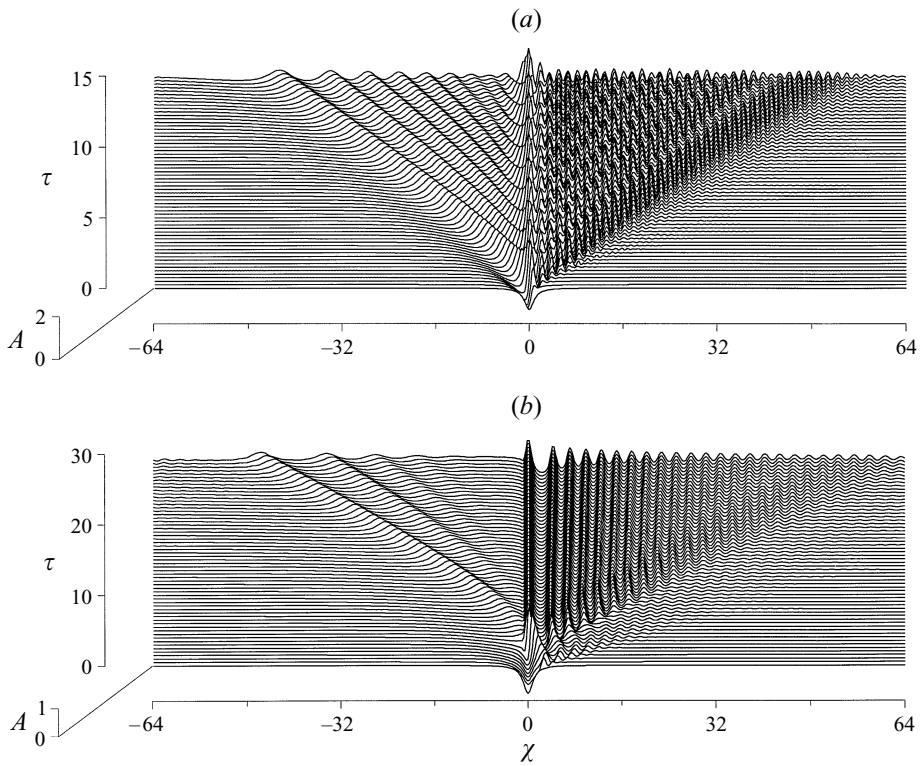


FIGURE 11. Two subcritical solutions of the fBDA equation, (33), and the topography (34): (a) small-amplitude solution where $\Delta = -4$ and $\alpha = 2$, and (b) large-amplitude solution where $\Delta = -2.5$ and $\alpha = 6$.

away upstream, an isolated wave forms at the outcrop and a lee-wave train forms downstream. As $|\Delta|$ increases and the flow becomes more subcritical the amplitude of the lee waves decreases and the flow becomes dominated by the isolated feature at the outcrop. The flows are once again unsteady in the small-amplitude subregime, due to precisely the wave generation mechanism identified in the blocked regime. This is clearest at and upstream of the outcrop; however modulation of the lee-wave train can also be seen, caused by small-amplitude waves propagating downstream. The subcritical linear unsteady solution falls into this subregime and the same unsteady behaviour throughout the domain is observed, due however explicitly to the initial

https://doi.org/10.1017/S0022112097005685 Published online by Cambridge University Press

dispersive wavetrain which decays as $O(\tau^{-1/2})$. The generation of waves immediately downstream of the topography is only seen once this wavetrain has decayed. In the large-amplitude subregime of figure 11(*b*) the flow at large time becomes steady at and downstream of the outcrop and small-amplitude waves form at the upstream edge as in the large-amplitude blocked subregime. Here, however, there is no permanent upstream influence.

One of the main features of the subcritical regime is that the undular bore propagates upstream and the forcing due to the obstacle has negligible influence on the evolution of the undular bore. In this regime and the supercritical regime, the features of the flow match to the large-Δ flow of §3, in which the evolution of the initial condition can be separated to leading order from the forcing.

7. Conclusions

This paper has presented results for the flow of a sheared coastal current past an outcropping of the coastal wall. It has been shown that hydraulically controlled flows cannot occur in this geometry. In the weakly nonlinear near-critical limit a forced BDA equation describes the evolution of the vorticity interface at the ocean edge of the current.

One question that arises from the analysis is whether there is any analogue of the hydraulic solutions that proved so accurate in other work on coastal currents (Haynes *et al.* 1993). The results here show that there exist two near-critical regimes: a blocked regime and a steady-critical regime. In the blocked regime solutions showing weak control at the outcrop are possible. These solutions feature a downstream shelf, weak upstream influence and a large-amplitude feature at the outcrop. Propagating waves are generated both upstream and downstream of the outcrop. In the steady-critical regime the flow becomes steady at large time with a large-amplitude feature at the obstacle, a periodic nonlinear wavetrain downstream and no upstream influence. For the topography (34), in terms of the three parameters of this system, μ, ϵ and U, introduced in §2, (64*a*) gives the steady-critical regime velocity band as

$$\mu - \left(\mu^2 + \tfrac{1}{2}\mu\epsilon\right)^{1/2} \leqslant U - 1 \leqslant 0, \tag{66}$$

while (65) gives the blocked band as

$$0 < U - 1 - \left(\mu^2 + \tfrac{1}{2}\mu\epsilon\right)^{1/2} \leqslant \mu. \tag{67}$$

The hydraulic limit corresponds to the limit $\mu \to 0$ for fixed ϵ. In this limit the blocked band is order μ, while the critical band is order $\mu^{1/2}$. Consequently, in the hydraulic limit both regimes vanish and the flows are simply supercritical or subcritical.

In all the solutions of Stern (1991) both the length and width of the outcrop are of the same order as the undisturbed shear-layer width, and so the results presented here cannot be directly compared with Stern's results. Nevertheless some general comparisons can be made. The blocked regime identified in §6 has the same characteristics as the blocking flows of Stern, with large-amplitude waves propagating upstream and a narrowing of the coastal current width downstream; however in the simulations presented here the large-amplitude waves always form on the downstream side of the topography, whereas in Stern's simulations the waves form on the upstream side. As the blocked band disappears in the hydraulic limit, the blocking is, as suggested by Stern, a weak hydraulic effect. For relatively small obstacles, in our notation $\epsilon \leqslant 1$, Stern considers only $U = 1$ and finds no evidence of

https://doi.org/10.1017/S0022112097005685 Published online by Cambridge University Press

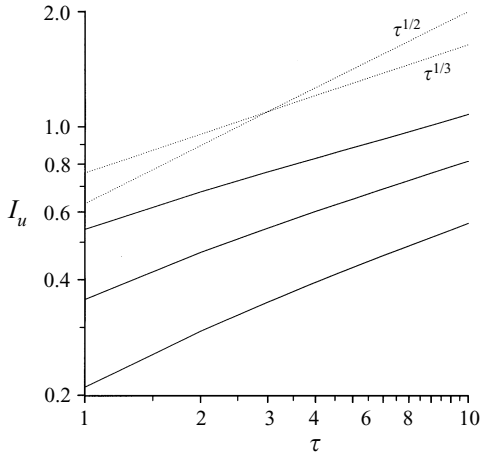


FIGURE 12. The evolution of the upstream area I_u, (68), for solutions of the fBDA equation, (33), with the topography (34), $\Delta = 0$ and $\alpha = 1, 2$ and 4, where I_u increases with α. Also shown as dotted lines for reference are $I_u \sim \tau^{1/2}$ and $I_u \sim \tau^{1/3}$.

blocking. The present results, showing that for weakly nonlinear waves the blocked band only occurs for $U < 1$, agree with this. For $U = 1$ and relatively small obstacles, Stern shows that the area of the perturbation to the upstream interface increases as order $t^{1/2}$ (see his figure 5). The upstream area perturbation at any time t can be written

$$I_u(t) = \int_{-\infty}^{0} \{A(x,t) - A(x,0)\}\,\mathrm{d}x. \tag{68}$$

Figure 12 gives the evolution of I_u when $\Delta = 0$ for $\alpha = 1, 2$ and 4. In each case the rate of increase of I_u decreases with time and for large time is order $\tau^{1/3}$, rather than order $\tau^{1/2}$. This is due to only long-wave effects being included in our analysis. The companion paper (Clarke & Johnson 1997) compares these contour dynamical simulations with a finite-amplitude generalization of the fBDA equation.

This work was carried out under grant number GR3/09174 from the Natural Environment Research Council. S.R.C. would like to thank the London Goodenough Trust for Overseas Graduates for helping make his stay in London possible.

Appendix. Solution of the steady fBDA equation

Solutions of (59) are sought using a Fourier transform relaxation method. In general the following method can be used to study periodic solutions, or isolated solutions where A approaches constant and equal limits in the far field. Here the approach for isolated solutions is described, where it is assumed that

$$\lim_{|\chi|\to\infty} A = 0. \tag{A 1}$$

The continuous function $A(\chi)$ is replaced by its value at N evenly spaced collocation points. Discrete Fourier transforms convert the operator $\mathscr{B}\{\ \}$ to a linear matrix B.

https://doi.org/10.1017/S0022112097005685 Published online by Cambridge University Press

Then (59) becomes the nonlinear system

$$\Delta A_j - \frac{\alpha}{2}A_j^2 + \sum_{k=1}^{N} B_{jk}(f_k + A_k) = 0, \qquad j = 1, \ldots, N. \tag{A 2}$$

This is solved straightforwardly with quadratic convergence using Newton's method with the initial choice $A_j \equiv 0$.

REFERENCES

Abramowitz, M. & Stegun, I. 1972 *Handbook of Mathematical Functions*, p. 232. US Dept. of Commerce.

Akylas, T. 1984 On the excitation of long nonlinear water waves by a moving pressure distribution. *J. Fluid. Mech.* **141**, 455–466.

Benjamin, T. 1967 Internal waves of permanent form in fluids of great depth. *J. Fluid Mech.* **29**, 559–592.

Clarke, S. & Johnson, E. 1997 Topographically forced long waves on a sheared coastal current. Part 2. Finite-amplitude waves. *J. Fluid Mech.* **343**, 153–168.

Davis, R. & Acrivos, A. 1967 Solitary internal waves in deep water. *J. Fluid Mech.* **29**, 593–607.

Fornberg, B. & Whitham, G. 1978 A numerical and theoretical study of certain nonlinear wave phenomena. *Phil. Trans. R. Soc. Lond.* A **289**, 373–404.

Grimshaw, R. 1987 Resonant forcing of barotropic coastally trapped waves. *J. Phys. Oceanogr.* **17**, 54–65.

Grimshaw, R. & Smyth, N. 1986 Resonant flow of a stratified fluid over topography. *J. Fluid Mech.* **169**, 429–464.

Haynes, P., Johnson, E. & Hurst, R. 1993 A simple model of Rossby-wave hydraulic behaviour. *J. Fluid Mech.* **253**, 359–384.

Hughes, R. 1985*a* Multiple criticalities in coastal flows. *Dyn. Atmos. Oceans* **9**, 321–340.

Hughes, R. 1985*b* On inertial currents over a sloping continental shelf. *Dyn. Atmos. Oceans* **9**, 49–73.

Hughes, R. 1986*a* On the conjugate behaviour of weak along-shore flows. *Tellus* **38A**, 227–284.

Hughes, R. 1986*b* On the role of criticality in coastal flows over irregular bottom topography. *Dyn. Atmos. Oceans* **10**, 129–147.

Hughes, R. 1987 The role of higher shelf modes in coastal hydraulics. *J. Mar. Res.* **45**, 33–58.

Hughes, R. 1989 The hydraulics of local separation in a coastal current, with application to the Kuriosho meander. *J. Phys. Oceanogr.* **19**, 1809–1820.

Johnson, E. 1985 Topographic waves and the evolution of coastal currents. *J. Fluid Mech.* **160**, 499–509.

Patoine, A. & Warn, T. 1982 The interaction of long, quasi–stationary waves with topography. *J. Atmos. Sci.* **39**, 1018–1025.

Pratt, L. & Armi, L. 1987 Hydraulic control of flows with nonuniform potential vorticity. *J. Phys. Oceanogr.* **19**, 81–106.

Pratt, L. & Lundberg, P. 1991 Hydraulics of rotating strait and sill flow. *Ann. Rev. Fluid Mech.* **23**, 81–106.

Stern, M. 1991 Blocking an inviscid shear flow. *J. Fluid Mech.* **227**, 449–472.

Woods, A. 1993 The topographic control of planetry-scale flow. *J. Fluid Mech.* **247**, 603–621.

https://doi.org/10.1017/S0022112097005685 Published online by Cambridge University Press